Available online at www.sciencedirect.com
SCIENCE DIRECT®
Journal of Computational Physics 196 (2004) 751–772
JOURNAL OF COMPUTATIONAL PHYSICS
www.elsevier.com/locate/jcp

Local discontinuous Galerkin methods for nonlinear dispersive equations

Doron Levy [a,*], Chi-Wang Shu [b], Jue Yan [c]

[a] Department of Mathematics, Stanford University, Stanford, CA 94305-2125, USA
[b] Division of Applied Mathematics, Brown University, Providence, RI 02912, USA
[c] Department of Mathematics, UCLA, Los Angeles, CA 90095, USA

Received 6 August 2003; received in revised form 29 October 2003; accepted 20 November 2003

Abstract

We develop local discontinuous Galerkin (DG) methods for solving nonlinear dispersive partial differential equations that have compactly supported traveling waves solutions, the so-called "compactons". The schemes we present extend the previous works of Yan and Shu on approximating solutions for linear dispersive equations and for certain KdV-type equations. We present two classes of DG methods for approximating solutions of such PDEs. First, we generate nonlinearly stable numerical schemes with a stability condition that is induced from a conservation law of the PDE. An alternative approach is based on constructing linearly stable schemes, i.e., schemes that are linearly stable to small perturbations. The numerical simulations we present verify the desired properties of the methods including their expected order of accuracy. In particular, we demonstrate the potential advantages of using DG methods over pseudo-spectral methods in situations where discontinuous fronts and rapid oscillations co-exist in a solution.

AMS: 65M60; 35Q53

Keywords: Discontinuous Galerkin; Compactons; Nonlinear dispersive equations; Stability

1. Introduction

In this paper, we are concerned with developing numerical approximations of solutions to nonlinear dispersive equations. The prototype of such equations is the $K(m,n)$ equation, introduced by Rosenau and Hyman in [16],

$$u_t + (u^m)_x + (u^n)_{xxx} = 0, \quad m > 0, 1 < n \leqslant 3.$$

* Corresponding author.
E-mail addresses: dlevy@math.stanford.edu (D. Levy), shu@dam.brown.edu (C.-W. Shu), yan@math.ucla.edu (J. Yan).

0021-9991/$ - see front matter
doi:10.1016/j.jcp.2003.11.013

For certain values of m and n, the $K(m,n)$ equation has compactly supported solitary waves solutions. These structures, the so-called *compactons*, have several things in common with soliton solutions of the Korteweg–de Vries (KdV) equation. For example, a single compacton moves with a velocity that is proportional to its amplitude; several compactons moving with different velocities and collide, will go through a nonlinear interaction from which they emerge with a phase shift; also, general initial data can break into a train of compactons. To illustrate the theoretical and numerical difficulties in treating compactons consider, e.g., the fundamental $K(2,2)$ compacton, which is of the form

$$u(x,t) = \begin{cases} \frac{4\lambda}{3}\left[\cos\left(\frac{x-\lambda t}{4}\right)\right]^2, & |x-\lambda t| \leqslant 2\pi, \\ 0, & \text{otherwise.} \end{cases}$$

In this case (which should be considered as a caricature of the general framework), the second derivatives do not exist on the edges of the compacton. Since the PDE involves a third derivative, it is necessary to interpret the $K(2,2)$ equation in a suitable weak sense. From such a point of view, there are some similarities between the $K(2,2)$ equation and, e.g., hyperbolic conservation laws. However, while a weak formulation of conservation laws leads to infinitely many weak solutions and hence one needs to use an additional condition in the form of an "entropy solution" to single out a unique solution, with the $K(2,2)$ equation (as well as with other similar equations), the situation is somewhat simpler. For example, one can add a constant to the solution, $u \to u + \alpha$ (which is equivalent to adding a linear dispersion term to the equation of the form αu_{xxx}). This transformation regularizes the solution, and the solution of the original equation can be obtained in a semi-classical sense by taking the limit $\alpha \to 0$. For more details we refer to [12–14]. For the purpose of the present work, we can therefore note that from an analytical point of view, solutions of compacton equations can be well defined, and from a numerical point of view, one has to be concerned about approximating solutions that have non-smooth interfaces. It is also important to stress that compactons do not develop only in the $K(m,n)$ equation. Compacton solutions were shown to exist for a variety of other nonlinear dispersive equations. For some examples, we refer to [12,13,15] and the references therein.

In this work we are interested in developing discontinuous Galerkin (DG) methods for approximating solutions of such nonlinear dispersive equations. First, we would like to comment on other approaches for approximating solutions for these equations. Most of the works concerning compactons (including [16]), use pseudo-spectral approximations. Unfortunately, to date, the stability and convergence properties of spectral methods for approximating solutions of such equations have not been studied. Moreover, with spectral methods, in order to eliminate the Gibbs oscillations that develop on the non-smooth interfaces of the solution, one has to use a filter, which might result in the removal of fine scales that can be part of the solution. A different approach was taken in [10,11], where certain finite-difference methods were explored. These methods generated instabilities on the interfaces. Recently, Chertock and Levy [2,3] used particle methods for approximating the solutions of compacton equations. Their method was based on the diffusion velocity particle method of Degond and Mustieles [9]. One advantage of particle methods over other methods is that it is relatively easy to preserve the sign of the solution. Hence, there is no need to worry about situations where the solution might change its sign and move into an ill-posed region of the equation due to spurious numerical oscillations. This is a relevant issue with some PDEs. This property of particle methods also plays against them when one is actually interested in solutions that can change their sign (which is often the case with dispersive equations).

The type of discontinuous Galerkin methods we will discuss in this paper, using a discontinuous Galerkin finite element approximation in the spatial variables coupled with explicit, nonlinearly stable high order Runge–Kutta time discretization [19], were first developed for conservation laws containing first derivatives by Cockburn and Shu [5,6]. For a detailed description of the method as well as its implementation and applications, we refer the readers to the lecture notes [4] and to the review paper [8].

For equations containing higher order spatial derivatives, discontinuous Galerkin methods cannot be directly applied. This is because the solution space, which consists of piecewise polynomials discontinuous at the element interfaces, is not regular enough to handle higher derivatives. This is a typical "non-conforming" case in finite elements. A naive and careless application of the discontinuous Galerkin method directly to the heat equation containing second derivatives could yield a method which behaves nicely in the computation but is inconsistent with the original equation suffering from O(1) errors [18,22].

The idea of local discontinuous Galerkin methods for time dependent PDEs with higher derivatives is to rewrite the equation as a first order system, and only then apply the discontinuous Galerkin method on the system. A key ingredient for the success of such methods is the careful design of interface numerical fluxes. These fluxes must be designed to guarantee stability and local solvability of all the auxiliary variables introduced to approximate the derivatives of the solution. The local solvability of all the auxiliary variables is why the method is called a "local" discontinuous Galerkin method in [7].

The first local discontinuous Galerkin method was developed by Cockburn and Shu [7], for a convection diffusion equation (containing second derivatives). Their work was motivated by the successful numerical experiments of Bassi and Rebay [1] for the compressible Navier–Stokes equations. Later, Yan and Shu [20] developed a local discontinuous Galerkin method for a general KdV type equation containing third derivatives. In both [7] and [20], suitable numerical fluxes at element interfaces were given, which led to provable nonlinear L^2 stability of the methods as well as error estimates for the linear cases. The LDG method was generalized to PDEs with fourth and fifth spatial derivatives in [21].

The structure of this paper is as follows. In Section 2 we present two formulations of our local DG method. We start in Section 2.1 with a review of stable DG methods for general KdV equations. Here we spell out the details of the formulation of DG schemes. We then proceed in Section 2.2 in which we extend these ideas to the $K(n,n)$ equation. In particular, we prove a nonlinear stability result showing that $\int u^{n+1}\,dx$ does not increase in time (which in the case of an odd power n is equivalent to saying that the L^{n+1}-norm of the solution does not increase in time). Finally, in Section 2.3 we present an alternative approach for the construction of the numerical fluxes in which we write a scheme that is stable with respect to small perturbations of the solution.

In Section 3 we present a series of numerical simulations in which we verify the expected accuracy of the scheme and check the stability by monitoring the L^p-norm for a suitable power. We also present several numerical experiments in which we show collisions between compactons and how compactons emerge from compact initial data. In particular, we present a couple of examples in which rapid oscillations develop behind the moving compactons. We demonstrate that unlike pseudo-spectral methods, our DG methods are capable of capturing simultaneously the oscillations and the non-smooth fronts. Some concluding remarks are provided in Section 4.

2. The numerical scheme: formulation and theoretical results

2.1. Generalized KdV equations

In [20], Yan and Shu presented and analyzed a local discontinuous Galerkin method for KdV-type equations of the form

$$u_t + f(u)_x + (r'(u)g(r(u)_x)_x)_x = 0, \tag{2.1}$$

augmented with the initial data $u(x,t=0) = u_0(x)$, and periodic boundary conditions. The functions $f(u), r(u)$, and $g(u)$ are arbitrary (smooth) functions. The KdV equation is a special case of (2.1) (for the choice $f(u) = u^2$, $g(u) = u$, and $r(u) = u$).

The form of Eq. (2.1) was chosen due to technical considerations: it turns to be a natural extension of the KdV equations that still allows one to write a stable DG method. Interestingly, it is not easy to find a model of interest with a nonlinear dispersive term that fits into the form of (2.1), which is the reason as of why no such examples were presented in [20].

It turns out that a model proposed in [17] does belong to the family of equations described by (2.1). For the choice $f(u) = u^3$, $r(u) = u^2$ and $g(u) = u/2$, we obtain

$$u_t + (u^3)_x + (u(u^2)_{xx})_x = 0. \tag{2.2}$$

Eq. (2.2) is known to have compacton solutions of the form

$$u(x,t) = \begin{cases} \sqrt{2\lambda}\cos\left(\frac{x-\lambda t}{2}\right), & |x-\lambda t| \leqslant \pi, \\ 0, & \text{otherwise.} \end{cases}$$

To make this presentation self-contained, we start with a brief description of a stable DG method for (2.1). We denote the mesh by $I_j = [x_{j-1/2}, x_{j+1/2}]$, for $j = 1, \ldots, N$. The center of the cell is $x_j = (x_{j-1/2} + x_{j+1/2})/2$, and $\Delta x_j = |I_j|$. We denote by $u^+_{j+1/2}$ and $u^-_{j+1/2}$ the value of u at $x_{j+1/2}$, from the right cell, I_{j+1}, and from the left cell, I_j, respectively. We can now define the piecewise-polynomial space $\mathscr{V}_{\Delta x}$ as the space of polynomials of degree k in each cell I_j, i.e.,

$$\mathscr{V}_{\Delta x} = \left\{v : \ v \in P^k(I_j) \text{ for } x \in I_j, \ j = 1, \ldots, N\right\},$$

Now, consider (2.1) on a periodic domain Ω and rewrite it as the first-order system

$$\begin{cases} u_t + (f(u) + r'(u)p)_x = 0, \\ p - g(q)_x = 0, \\ q - r(u)_x = 0. \end{cases} \tag{2.3}$$

We search for a solution of (2.3) in terms of piecewise polynomial functions, $u, p, q \in \mathscr{V}_{\Delta x}$, that satisfy (2.3) in a weak sense. Hence, we multiply (2.3) by test functions $v, w, z \in \mathscr{V}_{\Delta x}$, and integrate by parts in every cell I_j to obtain

$$\begin{aligned} &\int_{I_j} u_t v \,\mathrm{d}x - \int_{I_j} (f(u) + r'(u)p) v_x \,\mathrm{d}x + \left(\hat{f} + \widehat{r'}\hat{p}\right)_{j+\frac{1}{2}} v^-_{j+\frac{1}{2}} - \left(\hat{f} + \widehat{r'}\hat{p}\right)_{j-\frac{1}{2}} v^+_{j-\frac{1}{2}} = 0, \\ &\int_{I_j} pw \,\mathrm{d}x + \int_{I_j} g(q) w_x \,\mathrm{d}x - \hat{g}_{j+\frac{1}{2}} w^-_{j+\frac{1}{2}} + \hat{g}_{j-\frac{1}{2}} w^+_{j-\frac{1}{2}} = 0, \\ &\int_{I_j} qz \,\mathrm{d}x + \int_{I_j} r(u) z_x \,\mathrm{d}x - \hat{r}_{j+\frac{1}{2}} z^-_{j+\frac{1}{2}} + \hat{r}_{j-\frac{1}{2}} z^+_{j-\frac{1}{2}} = 0. \end{aligned} \tag{2.4}$$

The "hat" terms in (2.4) are the boundary terms that emerge from the integration by parts. These are the so-called "numerical fluxes" that are yet to be determined. The freedom in choosing numerical fluxes can be utilized for designing a scheme that enjoys certain stability properties. Indeed, it was shown in [20] that it is possible to prove a cell entropy inequality, an L^2-stability result and to obtain error estimates if these numerical fluxes are chosen as:

$$\begin{aligned} &\widehat{r'} = \frac{r(u^+) - r(u^-)}{u^+ - u^-}, \quad \hat{r} = r(u^-), \quad \hat{p} = p^+, \\ &\hat{f} = \hat{f}(u^-, u^+), \quad \hat{g} = \hat{g}(q^-, q^+). \end{aligned} \tag{2.5}$$

We omit the half-integer indices $j + 1/2$ as all quantities in (2.5) are computed at the same points (i.e., the interfaces between the cells). Here $\hat{f}(u^-, u^+)$ and $-\hat{g}(q^-, q^+)$ are monotone fluxes, i.e., Lipschitz con-

tinuous in both arguments, consistent (i.e., $\hat{f}(u,u) = f(u)$), non-decreasing in the first argument, and non-increasing in the second. With such a choice of fluxes, we have:

Proposition 2.1 (Cell entropy inequality). *There exist numerical entropy fluxes $\hat{H}_{j+1/2}$ such that the solution to the scheme* (2.4) *and* (2.5) *satisfies*

$$\frac{1}{2}\frac{\mathrm{d}}{\mathrm{d}t}\int_{I_j} u^2(x,t)\,\mathrm{d}x + \left(\hat{H}_{j+\frac{1}{2}} - \hat{H}_{j-\frac{1}{2}}\right) \leqslant 0. \tag{2.6}$$

The proof of Proposition 2.1 can be found in [20]. Next, by summing (2.6) over all j, we have:

Corollary 2.1 (L^2 stability). *The solution to the scheme* (2.4) *and* (2.5) *is L^2 stable, i.e.,*

$$\frac{1}{2}\frac{\mathrm{d}}{\mathrm{d}t}\int_{\Omega} u^2(x,t)\,\mathrm{d}x \leqslant 0.$$

Finally, we write the following error estimate, the proof of which can be found in [20].

Proposition 2.2 (Error estimate). *The error for the scheme* (2.4) *and* (2.5) *applied to the linear PDE*

$$v_t + v_x + v_{xxx} = 0$$

satisfies

$$\|e_v\|_{L^2} \leqslant C\Delta x^{k+1/2}, \tag{2.7}$$

where e_v is the difference between the smooth solution and its numerical approximation. The constant C depends on the first $k+3$ derivatives of v and the time t.

Remarks.

1. The choice of numerical fluxes in (2.5) is not unique. There is more than one way to choose these fluxes and obtain the stability results.
2. The numerical simulations hint that the error estimate (2.7) is sub-optimal. An order of $k+1$ is observed instead of the proved $k+1/2$ both in the L^2 and the L^∞ norms.
3. The proof of cell entropy inequality and L^2 stability could be easily extended to the multi-dimensional case. Numerically, an order of $k+1$ could be obtained for 2-D dispersive equations.
4. The stability results are valid not only for periodic boundary conditions. Stable schemes can be derived also for other types of boundary conditions.

2.2. The $K(n,n)$ equation – method I

Consider the $K(n,n)$ equation

$$u_t + (u^n)_x + (u^n)_{xxx} = 0, \tag{2.8}$$

augmented with initial data $u(x,t=0) = u_0(x)$, and periodic boundary conditions. In this section we write a local DG method for which we then prove that the integral of the $(n+1)$th power of the approximate solution, $\int u^{n+1}\,\mathrm{d}x$, does not increase in time. Later, we will present another method for approximating the solution of (2.8) which is based on linearization and compare the results obtained with both methods.

We start by rewriting (2.8) as a first order system, with three additional variables, v, p, q:

$$\begin{cases} u_t + (v+p)_x = 0, \\ p - q_x = 0, \\ q - v_x = 0, \\ v - u^n = 0, \end{cases} \tag{2.9}$$

and look for $u, v, p, q \in \mathscr{V}_{\Delta x}$, such that for all test functions $s, l, w, z \in \mathscr{V}_{\Delta x}$

$$\begin{aligned} &\int_{I_j} u_t s \,\mathrm{d}x - \int_{I_j} (v+p) s_x \,\mathrm{d}x + (\tilde{v}_{j+\frac{1}{2}} + \hat{p}_{j+\frac{1}{2}}) s^-_{j+\frac{1}{2}} - (\tilde{v}_{j-\frac{1}{2}} + \hat{p}_{j-\frac{1}{2}}) s^+_{j-\frac{1}{2}} = 0, \\ &\int_{I_j} p l \,\mathrm{d}x + \int_{I_j} q l_x \,\mathrm{d}x - \hat{q}_{j+\frac{1}{2}} l^-_{j+\frac{1}{2}} + \hat{q}_{j-\frac{1}{2}} l^+_{j-\frac{1}{2}} = 0, \\ &\int_{I_j} q w \,\mathrm{d}x + \int_{I_j} v w_x \,\mathrm{d}x - \hat{v}_{j+\frac{1}{2}} w^-_{j+\frac{1}{2}} + \hat{v}_{j-\frac{1}{2}} w^+_{j-\frac{1}{2}} = 0, \\ &\int_{I_j} v z \,\mathrm{d}x - \int_{I_j} u^n z \,\mathrm{d}x = 0. \end{aligned} \tag{2.10}$$

The numerical flux $\tilde{v}$ in the first equation in (2.10) is a convective flux, which we can choose in different ways such as, e.g., by upwinding. It still remains to determine the other numerical fluxes $\hat{p}$, $\hat{q}$, and $\hat{v}$ in (2.10). Since there is an explicit relation between p and v ($p = v_{xx}$), there really is only one degree of freedom in determining $\hat{p}$ and $\hat{v}$. In this case, $\hat{p}$ and $\hat{v}$ will have to be from opposite sides to guarantee stability. The stability analysis below suggests that an appropriate choice of these fluxes can be

$$\hat{p}_{j+\frac{1}{2}} = p^+_{j+\frac{1}{2}}, \quad \hat{q}_{j+\frac{1}{2}} = q^+_{j+\frac{1}{2}}, \quad \hat{v}_{j+\frac{1}{2}} = v^-_{j+\frac{1}{2}}, \tag{2.11}$$

or

$$\hat{p}_{j+\frac{1}{2}} = p^-_{j+\frac{1}{2}}, \quad \hat{q}_{j+\frac{1}{2}} = q^+_{j+\frac{1}{2}}, \quad \hat{v}_{j+\frac{1}{2}} = v^+_{j+\frac{1}{2}}. \tag{2.12}$$

Proposition 2.3. *The integral*

$$\int_\Omega u^{n+1} \,\mathrm{d}x,$$

where u is the solution of (2.10) *and* (2.11), *does not increase in time.*

Proof. We first assume that the power n is odd and choose an upwind convective flux, $\tilde{v}_{j+1/2} = v^-_{j+1/2}$. We comment on even powers in a remark following the proof. Since (2.10) holds for any test functions in $\mathscr{V}_{\Delta x}$, in particular we can choose $s = v$, $l = q$, $w = -p$, and $z = u_t$. With these test functions and the numerical fluxes of (2.11), Eq. (2.10) becomes

$$\begin{aligned} &\int_{I_j} u_t v \,\mathrm{d}x - \frac{1}{2}\int_{I_j} (v^2)_x \,\mathrm{d}x - \int_{I_j} p v_x \,\mathrm{d}x + (v^-_{j+\frac{1}{2}})^2 - v^-_{j-\frac{1}{2}} v^+_{j-\frac{1}{2}} + p^+_{j+\frac{1}{2}} v^-_{j+\frac{1}{2}} - p^+_{j-\frac{1}{2}} v^+_{j-\frac{1}{2}} = 0, \\ &\int_{I_j} p q \,\mathrm{d}x + \frac{1}{2}\int_{I_j} (q^2)_x \,\mathrm{d}x - q^+_{j+\frac{1}{2}} q^-_{j+\frac{1}{2}} + (q^+_{j-\frac{1}{2}})^2 = 0, \\ &-\int_{I_j} q p \,\mathrm{d}x - \int_{I_j} v p_x \,\mathrm{d}x + v^-_{j+\frac{1}{2}} p^-_{j+\frac{1}{2}} - v^-_{j-\frac{1}{2}} p^+_{j-\frac{1}{2}} = 0, \\ &\int_{I_j} (v - u^n) u_t \,\mathrm{d}x = 0. \end{aligned} \tag{2.13}$$

Adding the first three equations in (2.13) and summing over all j (taking into account the periodic boundary conditions), yield

$$\int_\Omega u_t v \, dx + \frac{1}{2} \sum_j \left[\left(v^-_{j+\frac{1}{2}} - v^+_{j+\frac{1}{2}} \right)^2 \right] + \frac{1}{2} \sum_j \left[\left(q^-_{j+\frac{1}{2}} - q^+_{j+\frac{1}{2}} \right)^2 \right] = 0.$$

Hence $\int_\Omega u_t v \, dx \leqslant 0$, and with the fourth equation in (2.13), we have:

$$\frac{d}{dt} \int_\Omega u^{n+1} \, dx \leqslant 0. \qquad \square$$

Remarks.

1. For an even power n, the same choice of $\tilde{v}$ gives a decay of $\int u^{n+1} \, dx$. However, this may not be a good choice in terms of upwinding and a truly upwind biased flux, such as the Lax–Friedrichs flux, should be used.
2. The result of the proposition still holds if the numerical fluxes are chosen as (2.12) instead of (2.11).
3. In case the power n is odd, Proposition 2.3 states that the L^{n+1}-norm of the solution does not increase in time. Hence, in the case where n is odd, Proposition 2.3 provides a stability result. For example, for the $K(3,3)$ equation, we end up with a scheme for which the L^4-norm of the solution does not increase in time. This is a more desirable situation as far as the stability of the scheme is concerned when compared, e.g., with the $K(2,2)$ equation for which all we get is that $\int u^3 \, dx$ does not decay in time, and hence, significantly less control over the numerical solution.
4. It is straightforward to extend the LDG method to other types of boundary conditions and to obtain similar stability results as long as the initial-boundary value problem is well-posed. This is one of the main advantages of finite element methods to which LDG belongs. Examples for different types of boundary conditions for LDG methods for the KdV equation can be found in [20]. Identical treatment of the boundary could also be applied to our case.

2.3. The $K(n,n)$ equation – method II

An alternative construction of the numerical flux can be done with linearization arguments. To demonstrate the main idea, we consider the $K(n,n)$ equation

$$u_t + (u^n)_x + (u^n)_{xxx} = 0, \tag{2.14}$$

augmented with the initial condition $u(x, t = 0) = u_0(x)$, and subject to periodic boundary conditions. In Section 2.2, we have constructed a scheme for which $\int u^{n+1} \, dx$, does not increase in time (here, u is the numerical solution). As already pointed out in a remark to Proposition 2.3, there is a difference between odd and even powers. Odd n's conserve an L^p-norm of an even power, which can be understood as a stability condition on the numerical solution. On the other hand, even n's, conserve $\int u^{n+1} \, dx$, with $(n+1)$ odd, in which case we have less control over the numerical solution.

In such cases, we would like to write a scheme that is at least stable with respect to small perturbations of the solution. We assume that $\bar{u}(x,t)$ is the exact solution of (2.14), and consider

$$u(x,t) = \bar{u}(x,t) + v(x,t), \tag{2.15}$$

where $v(x,t)$ is a small perturbation. Substituting (2.15) in (2.14) and neglecting high-order terms, we have

$$v_t + n(\bar{u}^{n-1} v)_x + n(\bar{u}^{n-1} v)_{xxx} = 0. \tag{2.16}$$

To further simplify (2.16) we set $\bar{u} = c$, for a constant c, and end up with

$$v_t + av_x + av_{xxx} = 0, \quad a = nc^{n-1}. \tag{2.17}$$

The next step is to write a stable numerical scheme for the linear equation (2.17). Here, by stability we mean that the L^2 norm of the numerical solution is non-increasing in time. This will provide us with a suitable choice of numerical fluxes which we can then generalize to finally obtain a scheme for the nonlinear equation (2.14). First, we rewrite (2.17) as the first-order system

$$\begin{cases} v_t + av_x + p_x = 0, \\ p - aq_x = 0, \\ q - v_x = 0, \end{cases} \tag{2.18}$$

and seek for $v, p, q \in \mathscr{V}_{\Delta x}$ such that for all test functions $s, l, w \in \mathscr{V}_{\Delta x}$, the following system is satisfied:

$$\begin{aligned} &\int_{I_j} v_t s \,\mathrm{d}x - \int_{I_j} (av + p) s_x \,\mathrm{d}x + (a\tilde{v}_{j+\frac{1}{2}} + \hat{p}_{j+\frac{1}{2}}) s^-_{j+\frac{1}{2}} - (a\tilde{v}_{j-\frac{1}{2}} + \hat{p}_{j-\frac{1}{2}}) s^+_{j-\frac{1}{2}} = 0, \\ &\int_{I_j} pl \,\mathrm{d}x + \int_{I_j} aql_x \,\mathrm{d}x - a\hat{q}_{j+\frac{1}{2}} l^-_{j+\frac{1}{2}} + a\hat{q}_{j-\frac{1}{2}} l^+_{j-\frac{1}{2}} = 0, \\ &\int_{I_j} qw \,\mathrm{d}x + \int_{I_j} vw_x \,\mathrm{d}x - \hat{v}_{j+\frac{1}{2}} w^-_{j+\frac{1}{2}} + \hat{v}_{j-\frac{1}{2}} w^+_{j-\frac{1}{2}} = 0. \end{aligned} \tag{2.19}$$

We need to specify $\tilde{v}, \hat{p}, \hat{q}$ and $\hat{v}$ (such that $\|v(t)\|_2$ is non-increasing). Here, $\tilde{v}$ is the convective flux, which can be chosen, e.g., as Lax–Friedrichs. The choice of the other numerical fluxes that will guarantee stability does depend on the sign of a. In case n is odd, a is always non-negative. However, if n is even, a can change its sign. For odd n we can either choose $\hat{p} = p^+,\ \hat{q} = q^+,\ \hat{v} = v^-$, or $\hat{p} = p^-,\ \hat{q} = q^+,\ \hat{v} = v^+$. For even n, it is easy to see that a (linearly) stable choice is:

$$\begin{aligned} &\hat{p} = p^-, \\ &\hat{q} = \begin{cases} q^+ & \text{if } a \geqslant 0, \\ q^- & \text{if } a < 0, \end{cases} \\ &\hat{v} = v^+. \end{aligned} \tag{2.20}$$

Now, given a scheme that is stable for the linear equation, the second step is to generalize it to the (nonlinear) $K(n,n)$ equation. Hence, we rewrite $K(n,n)$ as a first-order system:

$$\begin{cases} u_t + (u^n + p)_x = 0, \\ p - q_x = 0, \\ q - (u^n)_x = 0. \end{cases} \tag{2.21}$$

For odd n, the numerical fluxes are given as:

$$\begin{aligned} &\hat{p}_{j+\frac{1}{2}} = p^+_{j+\frac{1}{2}}, \\ &\hat{q}_{j+\frac{1}{2}} = q^+_{j+\frac{1}{2}}, \\ &\widehat{u^n}_{j+\frac{1}{2}} = (u^-_{j+\frac{1}{2}})^n \end{aligned}$$

(or $\hat{p} = p^-, \hat{q} = q^+, \widehat{u^n} = (u^+)^n$). For even n, the generalization of the linearly stable numerical fluxes reads:

$$\hat{p}_{j+\frac{1}{2}} = p^-_{j+\frac{1}{2}},$$
$$\hat{q}_{j+\frac{1}{2}} = \begin{cases} q^+_{j+\frac{1}{2}} & \text{if } (u^+_{j+\frac{1}{2}})^{n-1} + (u^-_{j+\frac{1}{2}})^{n-1} \geqslant 0, \\ q^-_{j+\frac{1}{2}}, & \text{otherwise,} \end{cases}$$
$$\widehat{u^n}_{j+\frac{1}{2}} = (u^+_{j+\frac{1}{2}})^n.$$

3. Numerical examples

The ODE solver we use in the following examples is the explicit, nonlinearly stable, third-order Runge–Kutta method of Shu and Osher [19]. Other ODE solvers can be used. In all examples, the figures present the solution obtained with a particular choice of grid. We have verified with the aid of successive mesh refinements, that in all cases, the approximations are numerically convergent.

3.1. A generalized KdV equation

In our first example, we approximate solutions of Eq. (2.2), $u_t + (u^3)_x + (u(u^2)_{xx})_x = 0$. First, in Table 1 we monitor the evolution of the L^2-norm of the solution for a single compacton initial data. Here, we use P^1 polynomials with 260 and 520 cells. As expected, the L^2-norm only decreases in time. Also, the finer the grid is, the slower is the rate of decay of the L^2-norm. In Table 2 we show an accuracy test for a single compacton initial data:

$$u(x,0) = \begin{cases} 2\cos(x/2), & x \in [-\pi, \pi], \\ 0, & \text{otherwise.} \end{cases} \tag{3.22}$$

The accuracy is measured away from the interface in the interval $[0, \pi]$ at $T = \pi/4$.

Table 1
The L^2-norm at different times for Eq. (2.2) and a single compacton initial data (3.22)

L^2 norm	$T = 0$	$T = 1$	$T = 2$	$T = 3$	$T = 4$	$T = 5$	$T = 6$	$T = 8$
$n = 260$	0.8779	0.8734	0.8702	0.8671	0.8640	0.8611	0.8582	0.8524
$n = 520$	0.8773	0.8744	0.8731	0.8725	0.8718	0.8712	0.8706	0.8695

The solution is obtained with the L^2-stable scheme of Section 2.1 and P^1 polynomials.

Table 2
An accuracy test for Eq. (2.2) with a one-compacton initial data (3.22)

k		$N = 48$	$N = 80$		$N = 112$		$N = 144$	
		Error	Error	Order	Error	Order	Error	Order
0	L^2	1.97e−01	1.45e−01	0.60	1.16e−01	0.68	9.62e−02	0.73
	L^∞	4.83e−01	3.54e−01	0.61	2.81e−01	0.68	2.34e−01	0.73
1	L^2	1.35e−03	5.46e−04	1.77	2.76e−04	2.01	1.79e−04	1.71
	L^∞	7.96e−03	2.99e−03	1.92	1.70e−03	1.66	1.07e−03	1.84

The computational domain is $[-3\pi/2, 5\pi/2]$. The accuracy is computed for the compacton in smooth areas, at time $T = \pi/4$.

We proceed by showing a collision between two compactons in Fig. 1. The initial data are taken as

$$u(x,0) = \begin{cases} 4\cos((x+\pi)/2), & x \in [-2\pi, 0], \\ 2\cos((x-2\pi)/2), & x \in [\pi, 3\pi], \\ 0, & \text{otherwise.} \end{cases} \tag{3.23}$$

The computational domain is taken as $[-4\pi, 22\pi]$ with P^1 polynomials and 260 cells. The solution is shown at times $T = 1, 2, 4, 6$. As can be seen in the figure, there is some residue in this collision that seems to be of the form of a compacton–anti-compacton pair similar to the one reported for the $K(2,2)$ equation in [16]. In the next example we experiment with a collision between three compactons. The results are shown in Fig. 2. This time the initial data are taken as

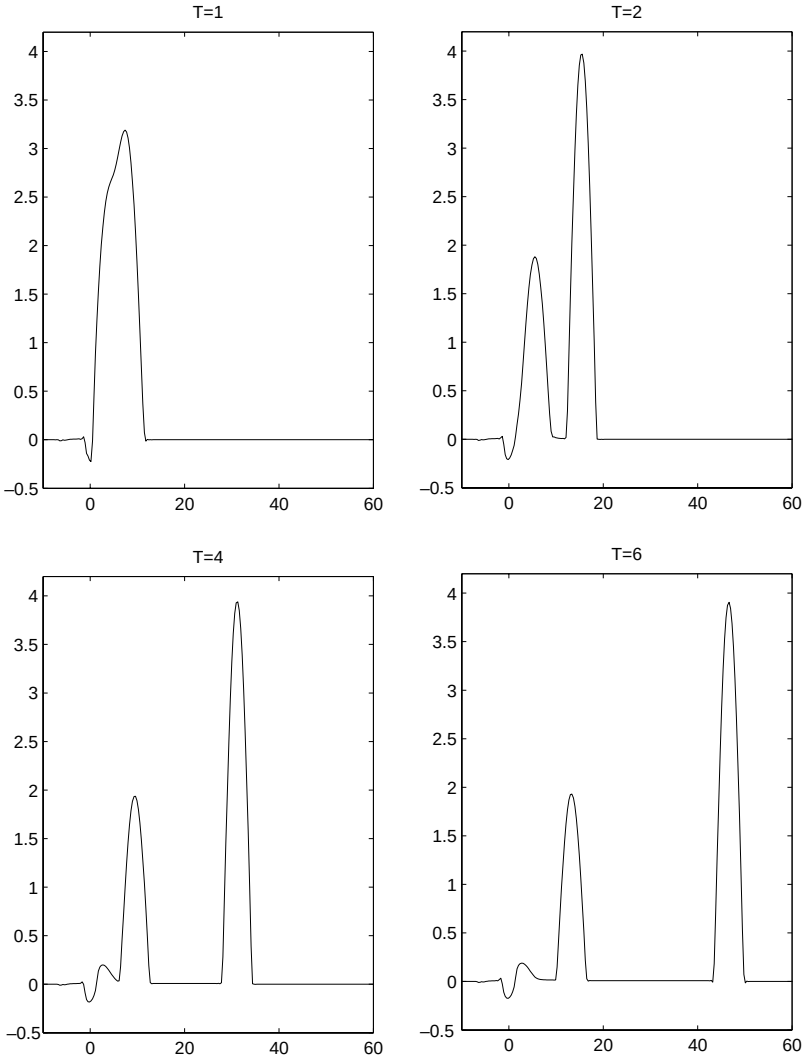

Fig. 1. An interaction between two compactons for Eq. (2.2). The initial data are given by (3.23). The solution is obtained with the L^2-stable scheme of Section 2.1. The polynomials are P^1 with 260 cells.

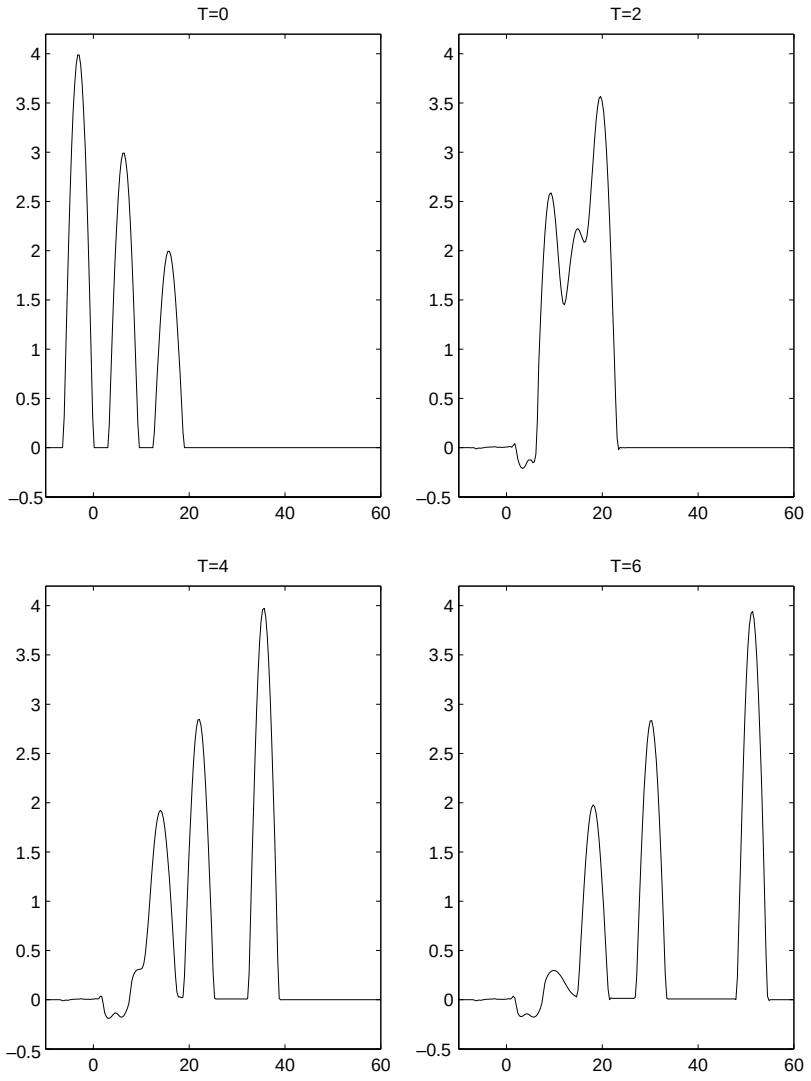

Fig. 2. An interaction between three compactons for equation (2.2). The initial data are given by (3.24). The solution is obtained with the L^2-stable scheme of Section 2.1. The polynomials are P^1 with 260 cells.

$$u(x,0) = \begin{cases} 4\cos((x+\pi)/2), & x \in [-2\pi, 0], \\ 3\cos((x-2\pi)/2), & x \in [\pi, 3\pi], \\ 2\cos((x-5\pi)/2), & x \in [4\pi, 6\pi], \\ 0, & \text{otherwise}. \end{cases} \tag{3.24}$$

Similarly to the previous example, the computational domain is taken as $[-4\pi, 22\pi]$ with P^1 polynomials and 260 cells. The solution is shown at times $T = 0, 2, 4, 6$. In this case there is also a residue in this collision, this time of an unknown structure.

3.2. The L^4-stable scheme for $K(3,3)$

In the following series of examples we present results obtained with the method described in Section 2.2. We start with checking the accuracy of the method by approximating the solution of the $K(3,3)$ equation

$$u_t + (u^3)_x + (u^3)_{xxx} = 0, \tag{3.25}$$

with a single compacton initial data of the form

$$u_0(x) = \begin{cases} \sqrt{\frac{3}{2}}\cos\left(\frac{x}{3}\right), & x \in [-1.5\pi, 1.5\pi], \\ 0, & \text{otherwise.} \end{cases} \tag{3.26}$$

The results are shown in Table 3. The accuracy is measured away from the interface in the interval $[0, 2\pi]$ at $T = \pi$. The degree of the polynomials is taken as $k = 0, 1$, and the results confirm the expected $k + 1$ order of accuracy of the scheme.

We proceed by exploring the interaction between two compactons. Here, the initial data are taken as

$$u_0(x) = \begin{cases} \sqrt{3}\cos(x), & x \in [-1.5\pi, 1.5\pi], \\ \sqrt{3/2}\cos(x - 3.5\pi), & x \in [2\pi, 5\pi], \\ 0, & \text{otherwise.} \end{cases} \tag{3.27}$$

The results are shown in Fig. 3. In particular, the solution is plotted during the nonlinear interaction at time $T = 6$, and after the compactons pass through each other at time $T = 20$. The polynomials are P^1 with 200 cells. As can be seen in the figure, the interaction leaves a small residue on the left side, so that the collision is not fully elastic. The compactons, however, do seem to emerge out of the interaction intact. Again, the residue of the interaction looks like a compacton–anti-compacton pair.

Next, we solve (3.25) subject to the initial data

$$u_0(x) = \sqrt{\frac{3}{2}}\cos\left(\frac{x}{6}\right), \quad x \in [-3\pi, 3\pi], \tag{3.28}$$

and zero elsewhere. The results of our simulations are shown in Fig. 4. As time evolves, a train of canonical compactons splits from the initial data and moves to the right. At the same time, a rapid oscillation develops at the left interface of the initial data. This example clearly demonstrates the advantages of the discontinuous Galerkin method over a pseudo-spectral method. In pseudo-spectral methods, one needs to

Table 3
An accuracy test for a one-compacton solution of the $K(3,3)$ equation (3.25) with a single compacton initial data (3.26)

k		$N = 40$	$N = 80$		$N = 160$		$N = 320$	
		Error	Error	Order	Error	Order	Error	Order
0	L^2	1.48 e − 01	9.22 e − 02	0.68	5.28 e − 02	0.80	2.84 e − 02	0.89
	L^∞	2.17 e − 01	1.35 e − 01	0.69	7.65 e − 02	0.82	4.10 e − 02	0.90
1	L^2	1.70 e − 03	3.92 e − 04	2.11	1.08 e − 04	1.85	2.65 e − 05	2.03
	L^∞	5.94 e − 03	1.70 e − 03	1.81	4.17 e − 04	2.02	1.01 e − 04	2.05

The solution is obtained with the L^4-stable scheme of Section 2.2. The computational domain is $[-2\pi, 3\pi]$. The accuracy is computed for the compacton in smooth areas. A $(k + 1)$ order of accuracy is observed.

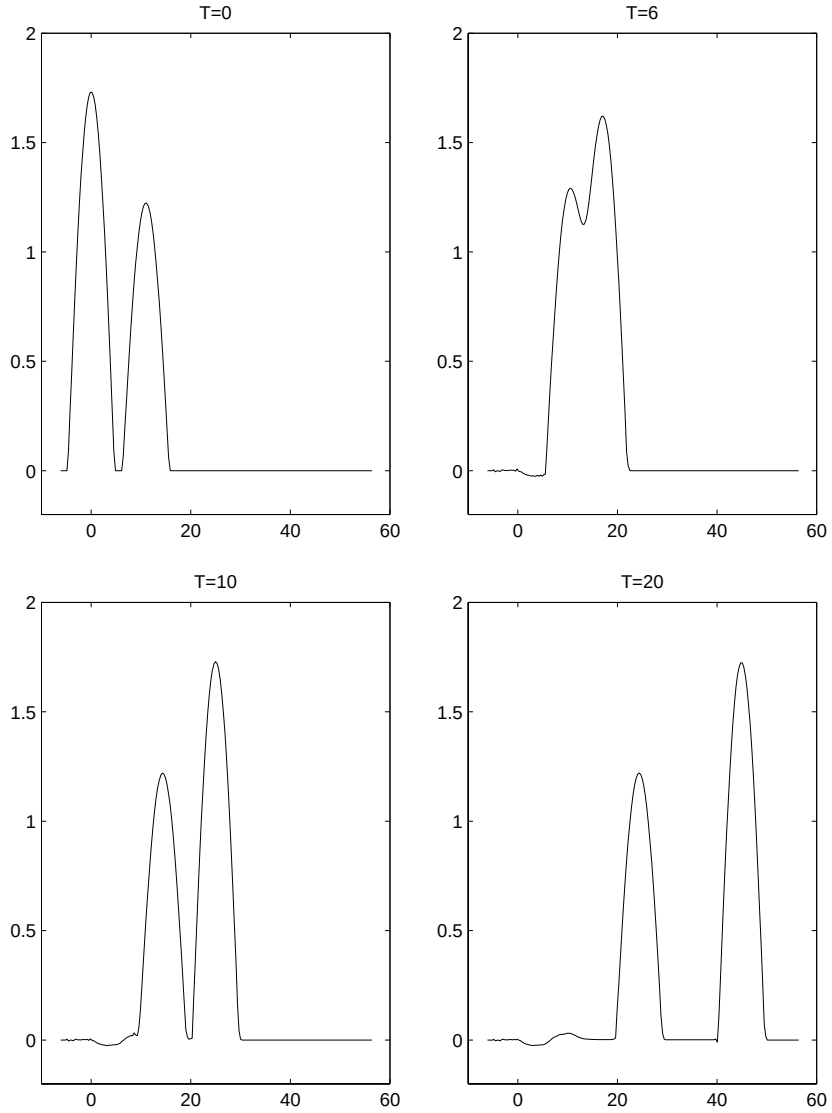

Fig. 3. An interaction between two compactons for the $K(3,3)$ equation (3.25). The initial data are given by (3.27). The solution is obtained with the L^4-stable scheme of Section 2.2. The polynomials are P^1 with 200 cells.

utilize a filter in order to remove the Gibbs oscillations that develop in the non-smooth interface (i.e., the edges of the compactons). In the Fourier space, a filter amounts to generating a (preferably) smooth decay in the high-modes. Unfortunately, such a filter can not distinguish between numerical oscillations that develop due to the non-smooth boundary, and physical oscillations, like the one that seems to develop in the present example on the left interface. We do not know what is the source of these oscillations, and to our knowledge, this is the first time that such oscillations are observed. Nevertheless, we consider this to be a fundamental example that shows how one method can capture simultaneously sharp interfaces and rapid oscillations without any special adaptation.

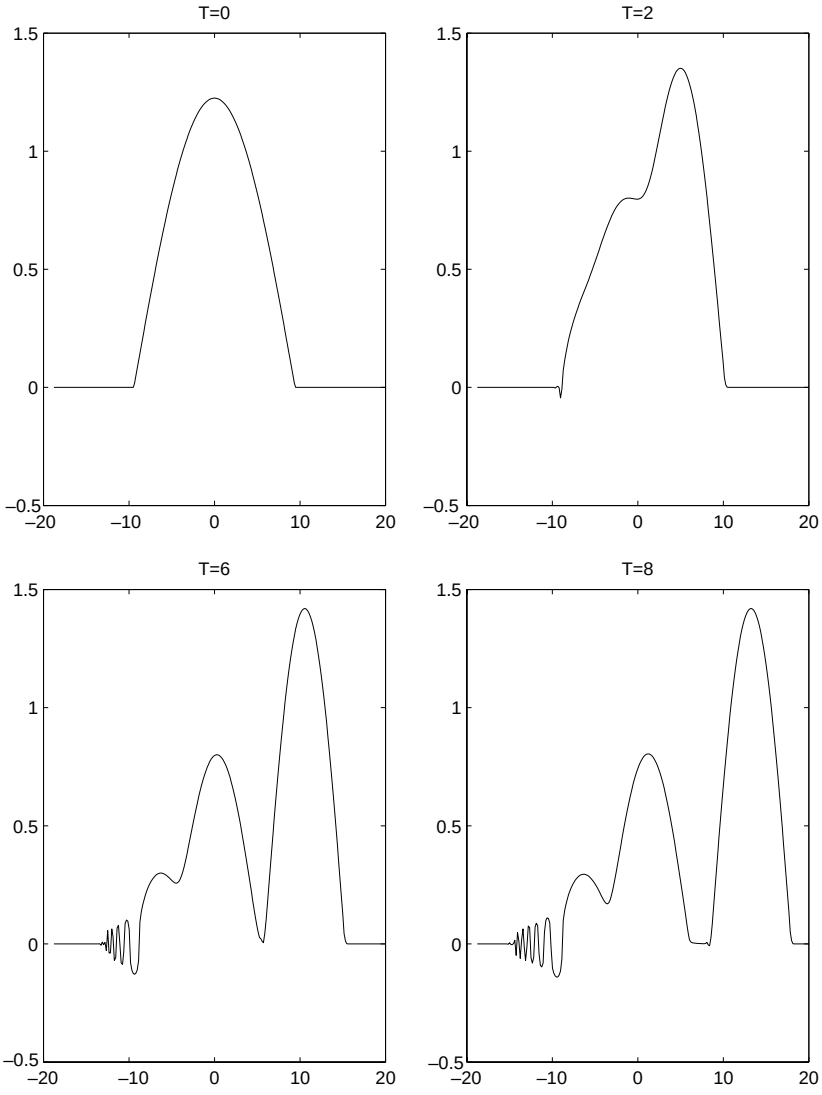

Fig. 4. The $K(3,3)$ equation (3.25). Compactons splitting from the initial data (3.28). Singular oscillations develop at the left interface. The solution is obtained with the L^4-stable scheme of Section 2.2. The polynomials are P^1 with 400 cells.

In Fig. 5 we compare the results of our DG method with those obtained with a pseudo-spectral method which is widely used in compacton computations. In order to be able to deal with the non-smooth interfaces with a pseudo-spectral method, we use a smooth low-pass filter in the Fourier space. While almost completely eliminating the Gibbs phenomenon away from the discontinuity, the filter does cause a noticeable damping in the oscillations at the left interface. A zoom on the oscillatory region is shown in Fig. 5(b). Even 1024 modes in a pseudo-spectral solution do not resolve the oscillations the way the DG method does with only 400 cells. Mesh refinements of the DG solution as well as an approximation that is obtained with P_2 polynomials are shown in Fig. 6. We believe that the similar oscillations that we get on the left side of the solution with two independent methods are a strong indication that the oscillations are an integral part of

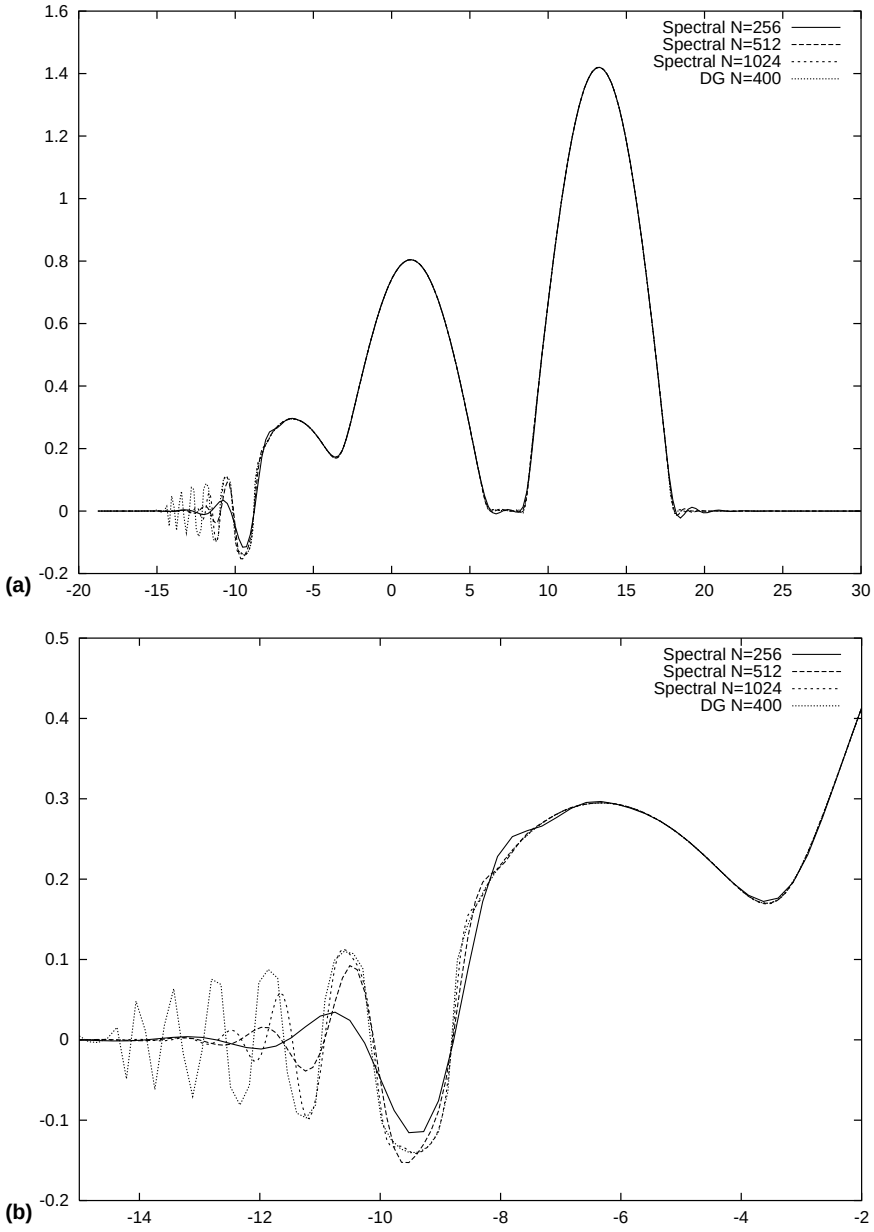

Fig. 5. The $K(3,3)$ equation (3.25). (a) Compactons splitting from the initial data (3.28) at $T = 8$. A solution obtained with a pseudo-spectral method (including a smooth high-pass filter) with $N = 256, 512, 1024$ modes. The DG method is the L^4-stable scheme of Section 2.2 with $N = 400$. (b) Zooming on the oscillatory region on the left interface.

the solution and not a numerical artifact. In Table 4 we monitor the L^4-norm of the computed solution at different times with different grid resolutions for the initial data (3.28). Clearly, there is a very slow decay of the L^4 norm in time, which confirms the stability properties of our scheme even when the solution is very oscillatory.

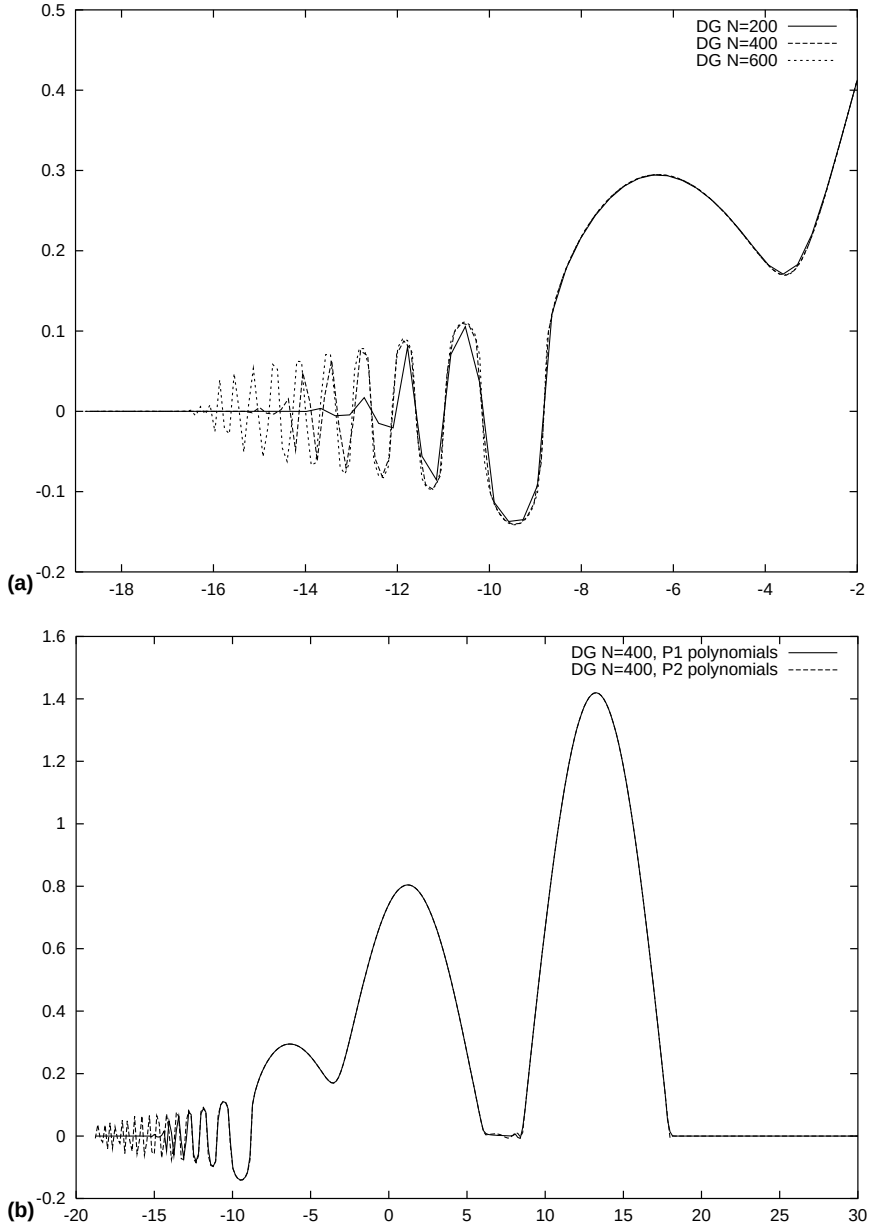

Fig. 6. The $K(3,3)$ equation (3.25). Compactons splitting from the initial data (3.28) at $T = 8$. A solution obtained with the L^4-stable DG scheme of Section 2.2 with (a) $N = 200, 400, 600$ with P^1 polynomials. (b) $N = 400$ with P^1 and P^2 polynomials.

Table 4
The L^4-norm for the $K(3,3)$ equation (3.25) with the initial data (3.28)

n	$T = 0$	$T = 2$	$T = 4$	$T = 6$	$T = 8$
300	0.70934	0.70933	0.70929	0.70923	0.70917
600	0.70932	0.70932	0.70931	0.70930	0.70930

The solution is obtained with the L^4-stable scheme of Section 2.2. The polynomials are P^1, with 300 and 600 points.

A somewhat similar phenomenon is observed when solving (3.25) subject to the initial data

$$u_0(x) = \begin{cases} 2\cos(x/5), & x \in [-2.5\pi, 2.5\pi], \\ 0, & \text{otherwise.} \end{cases} \tag{3.29}$$

The results are shown in Fig. 7. Here, we see compactons that split from the initial data and move to the right. At the same time, an oscillatory behavior develops at the left interface.

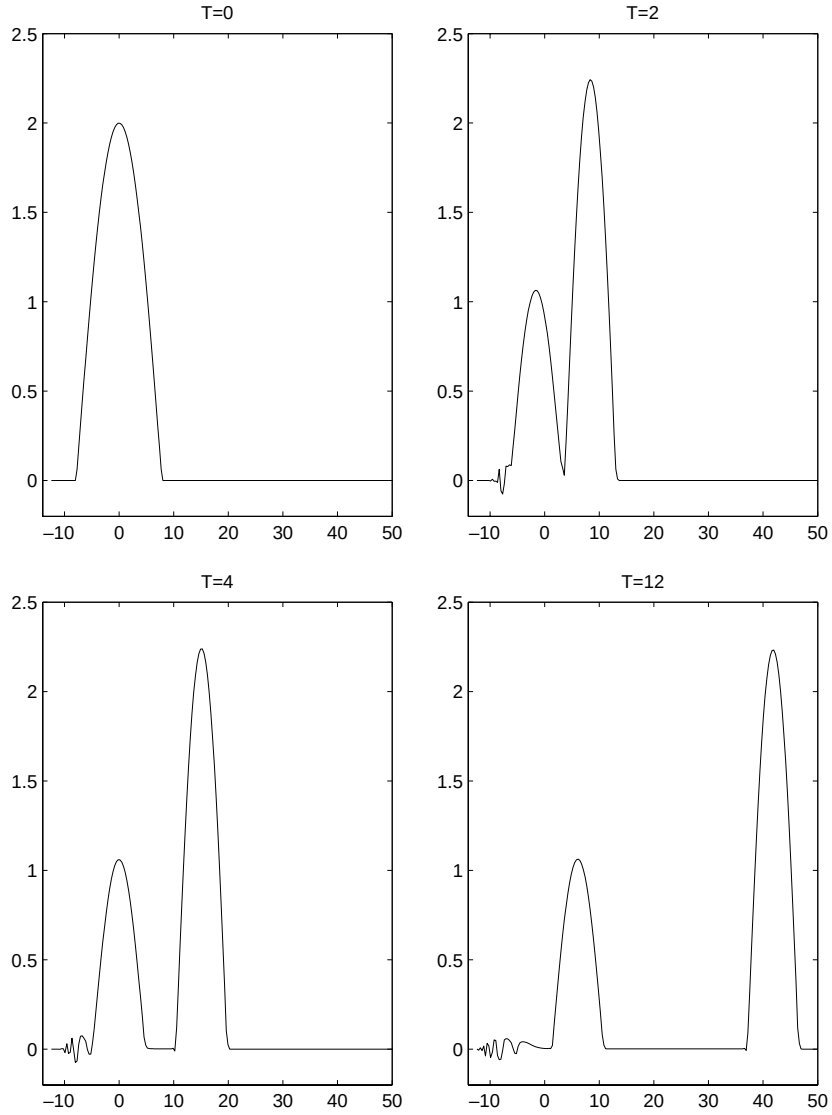

Fig. 7. The $K(3,3)$ equation (3.25). Compactons splitting from the initial data (3.29). Oscillations develop at the left interface. The solution is obtained with the L^4-stable scheme of Section 2.2. The polynomials are P^1 with 200 cells.

3.3. The linearly stable scheme for $K(2,2)$ and $K(3,3)$

In the following examples, we want to check the performance of the linearly stable schemes we developed in Section 2.3.

1. *The $K(2,2)$ equation.* The canonical traveling wave solution for the $K(2,2)$ equation,

$$u_t + (u^2)_x + (u^2)_{xxx} = 0, \tag{3.30}$$

is given by the compacton

$$u(x,t) = \frac{4\lambda}{3}\cos^2\left(\frac{x-\lambda t}{4}\right), \quad |x-\lambda t| \leqslant 2\pi. \tag{3.31}$$

In our first example, we solve (3.30) subject to a one-compacton initial condition (given by (3.31) with $\lambda = 1$). The results of the accuracy test with this initial data are shown in Table 5. The accuracy is measured away from the interface in the interval $[0, 2\pi]$. The accuracy is computed at $T = \pi/2$ with P^0, P^1 and P^2 polynomials. The results shown in this table confirm the expected $k+1$ order of accuracy.

A collision between two compactons is shown in Fig. 8. Similarly to the original compactons paper [16], after the collision we observe the emergence of a compacton–anti-compacton pair. Finally, compactons splitting from a more general initial data are shown in Fig. 9. Here, the initial data are taken as

$$u_0(x) = \frac{4}{3}\cos^2\left(\frac{x}{8}\right), \quad x \in [-4\pi, 4\pi], \tag{3.32}$$

and zero elsewhere.

2. *The $K(3,3)$ equation.* We would like to compare the L^4-stable scheme of Section 2.2 with the linearly stable scheme of Section 2.3. For that purpose, we repeat two of the previous examples: the interaction between two compactons with the initial data given by (3.27) and the compactons splitting from the initial data (3.28) (i.e., the example that develops the singular oscillations). The results of the simulations are shown in Fig. 10. In the first case with the two colliding compactons, the results obtained with both methods are nearly identical. With the second case, there is some difference between the solutions in the oscillatory region. The L^4-stable method seems to better resolve the oscillations.

Table 5
Order of accuracy for the $K(2,2)$ equation (3.30) with a one-compacton initial data (3.31), $\lambda = 1$, $T = \pi/2$

k		$N = 40$	$N = 80$		$N = 120$		$N = 160$	
		Error	Error	Order	Error	Order	Error	Order
0	L^2	7.32 e − 02	4.27 e − 02	0.78	3.01 e − 02	0.86	2.33 e − 02	0.90
	L^∞	2.30 e − 01	1.38 e − 01	0.73	9.84 e − 02	0.84	7.64 e − 02	0.88
1	L^2	1.55 e − 03	4.05 e − 04	1.94	1.83 e − 04	1.95	1.04 e − 04	1.97
	L^∞	1.21 e − 02	3.24 e − 03	1.90	1.47 e − 03	1.95	8.34 e − 04	1.96
2	L^2	1.14 e − 04	2.11 e − 05	2.43	4.49 e − 06	3.82	1.49 e − 06	3.83
	L^∞	6.04 e − 04	1.34 e − 04	2.19	2.62 e − 05	4.02	1.08 e − 05	3.07

The solution is obtained with the linearly stable scheme of Section 2.3. The computational domain is $[-4\pi, 4\pi]$. The accuracy is computed in a smooth region away from the interfaces.

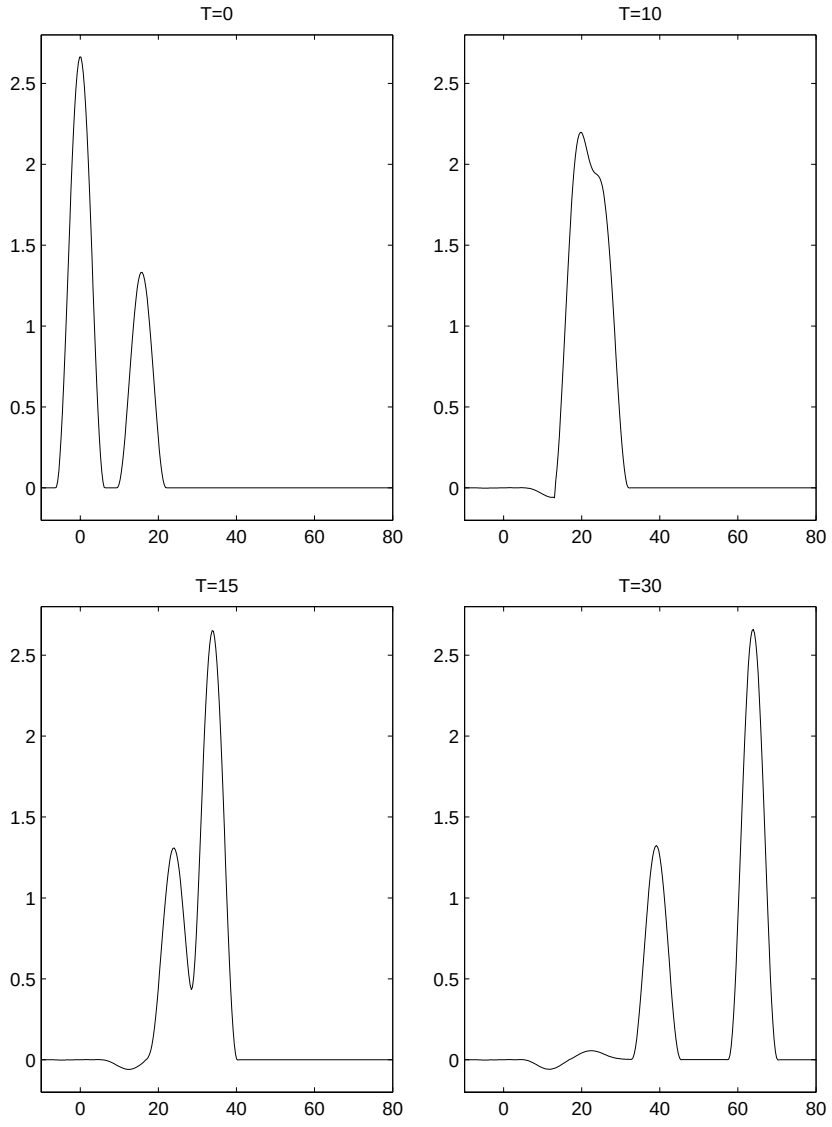

Fig. 8. Two compacton colliding for the $K(2,2)$ equation (3.30). The solution is obtained with the linearly stable scheme of Section 2.3. The polynomials are P^1 with 300 cells in $[-4\pi, 26\pi]$.

4. Conclusions

In this work we presented several approaches for designing numerical schemes for approximating solutions of certain nonlinear dispersive equations. First, in Section 2.2 we constructed a local DG method such that a conservation law for the equation was translated into a stability condition for the numerical scheme. While demonstrating this approach by supplying a suitable numerical flux for several equations of interest, it is important to note that this approach requires to carefully design the numerical flux that will suit the problem in hand.

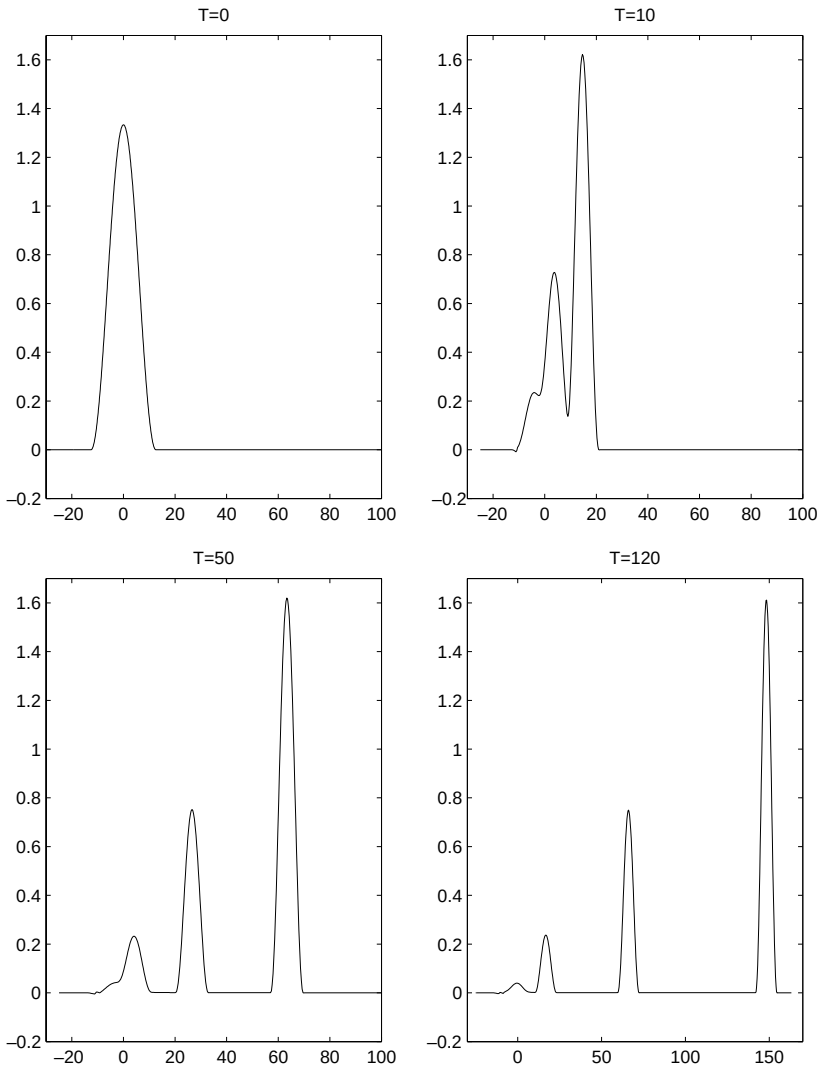

Fig. 9. Compactons splitting from general initial data in the $K(2,2)$ equation (3.30). The solution is obtained with the linearly stable scheme of Section 2.3. The initial data are given by (3.32). Note the different axis at $T = 120$.

In our second approach, the one of Section 2.3, we constructed a local DG method that is stable with respect to small perturbations of the solution. While providing less control over the numerical solution than the nonlinearly stable scheme of Section 2, the design of such linearly stable DG schemes for different equations is a relatively straightforward task.

Acknowledgements

We thank Xiaobing Feng, Hailiang Liu, and Philip Rosenau for fruitful discussions. The work of D. Levy was supported in part by the NSF under Career Grant DMS-0133511. The work of C.-W. Shu was

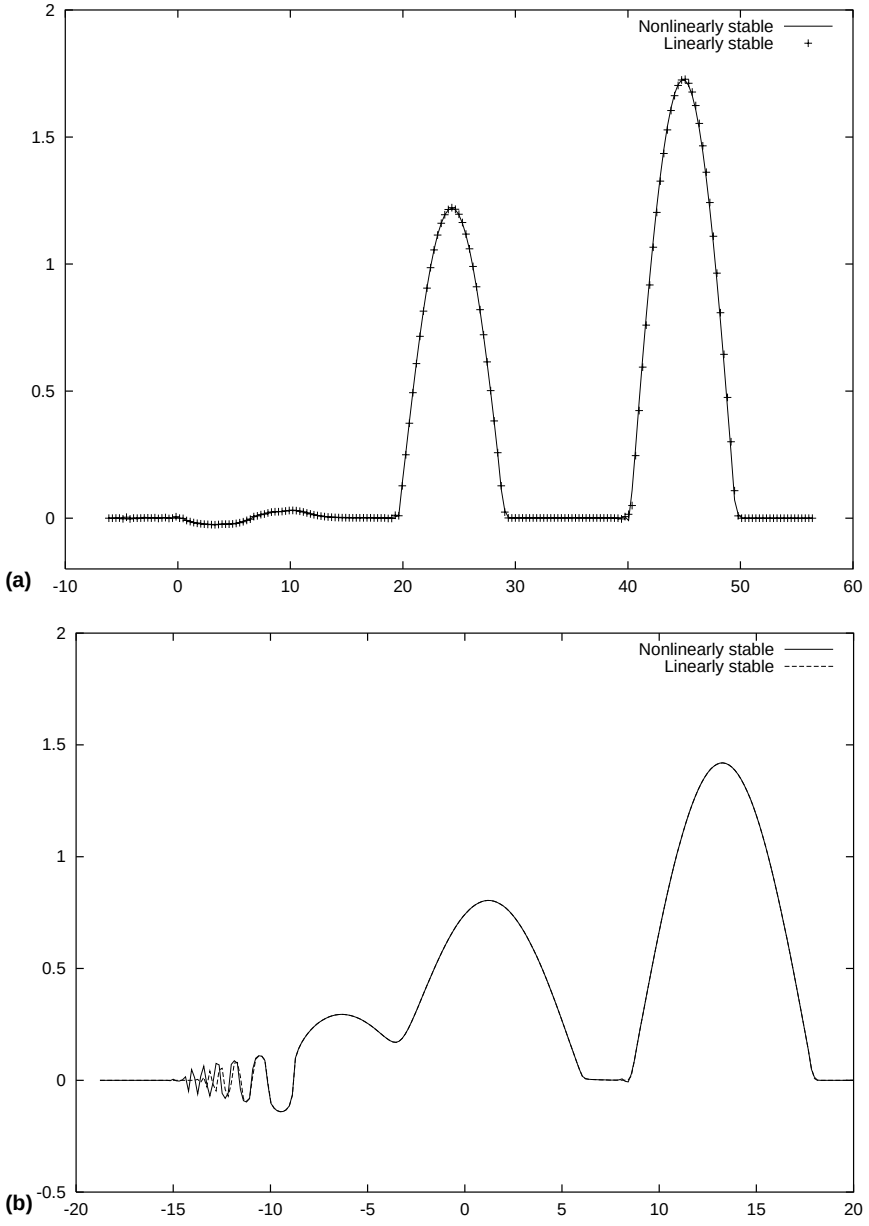

Fig. 10. The $K(3,3)$ equation (3.25). A comparison between the nonlinearly stable method of Section 2.2 and the linearly stable method of Section 2.3. (a) Two colliding compactons. The polynomials are P^1 with 200 cells in $[-2\pi, 18\pi]$ at $T = 20$. (b) Compactons splitting from the initial data (3.28) at $T = 8$. The polynomials are P^1 with 400 cells in $[-6\pi, 14\pi]$.

supported in part by ARO Grant DAAD19-00-1-0405, NSF Grant DMS-0207451, NASA Langley Grant NCC1-01035, and AFOSR Grant F49620-02-1-0113. The work of J. Yan was supported in part by ONR Grant N00014-02-1-0720.

References

[1] F. Bassi, S. Rebay, A high-order accurate discontinuous finite element method for the numerical solution of the compressible Navier–Stokes equations, J. Comput. Phys. 131 (1997) 267–279.
[2] A. Chertock, D. Levy, Particle methods for dispersive equations, J. Comput. Phys. 171 (2) (2001) 708–730.
[3] A. Chertock, D. Levy, A particle method for the KdV equation, in: Proceedings of the Fifth International Conference on Spectral and High Order Methods (ICOSAHOM-01) (Uppsala), J. Sci. Comput. 17 (1–4) (2002) 491–499.
[4] B. Cockburn, Discontinuous Galerkin methods for convection-dominated problems, in: T.J. Barth, H. Deconinck (Eds.), High-order Methods for Computational Physics, Lecture Notes in Computational Science and Engineering, vol. 9, Springer, Berlin, 1999, pp. 69–224.
[5] B. Cockburn, C.-W. Shu, TVB Runge–Kutta local projection discontinuous Galerkin finite element method for scalar conservation laws II: General framework, Math. Comp. 52 (1989) 411–435.
[6] B. Cockburn, C.-W. Shu, TVB Runge–Kutta local projection discontinuous Galerkin finite element method for scalar conservation laws V: Multidimensional systems, J. Comput. Phys. 141 (1998) 199–224.
[7] B. Cockburn, C.-W. Shu, The local discontinuous Galerkin method for time-dependent convection diffusion systems, SIAM J. Numer. Anal. 35 (1998) 2440–2463.
[8] B. Cockburn, C.-W. Shu, Runge–Kutta discontinuous Galerkin methods for convection-dominated problems, J. Sci. Comp. 16 (2001) 173–261.
[9] P. Degond, F.J. Mustieles, A deterministic approximation of diffusion equations using particles, SIAM J. Sci. Statist. Comp. 11 (2) (1990) 293–310.
[10] J. de Frutos, M.A. López-Marcos, J.M. Sanz-Serna, A finite difference scheme for the $K(2,2)$ compacton equation, J. Comput. Phys. 120 (1995) 248–252.
[11] M.S. Ismail, T.R. Taha, A numerical study of compactons, Math. Comput. Simul. 47 (1998) 519–530.
[12] Y.A. Li, P.J. Olver, Convergence of solitary-wave solutions in a perturbed Bi-Hamiltonian dynamical system: I. Compactons and peakons, Discrete Cont. Dyn. Syst. 3 (3) (1997) 419–432.
[13] Y.A. Li, P.J. Olver, Convergence of solitary-wave solutions in a perturbed Bi-Hamiltonian dynamical system. II. Complex analytic behavior and convergence to non-analytic solutions, Discrete Cont. Dyn. Syst. 4 (1998) 159–191.
[14] Y.A. Li, P.J. Olver, P. Rosenau, Non-analytic solutions of nonlinear wave models, in: Nonlinear Theory of Generalized Functions (Vienna, 1997) Chapman & Hall/CRC Press, Boca Raton, FL; Res. Notes Math., vol. 401, Chapman & Hall/CRC Press, Boca Raton, FL, 1999, pp. 129–145.
[15] P. Rosenau, Compact and noncompact dispersive patterns, Phys. Lett. A 275 (2000) 193–203.
[16] P. Rosenau, J.M. Hyman, Compactons: solitons with finite wavelength, Phys. Rev. Lett. 70 (5) (1993) 564–567.
[17] P. Rosenau, D. Levy, Compactons in a class of nonlinearly quintic equations, Phys. Lett. A 252 (1999) 297–306.
[18] C.-W. Shu, Different formulations of the discontinuous Galerkin methods for the viscous terms, in: Z.-C. Shu, M. Mu, W. Xue, J. Zou (Eds.), Advances in Scientific Computing, Science Press, Moscow, 2001, pp. 144–155.
[19] C.-W. Shu, S. Osher, Efficient implementation of essentially non-oscillatory shock capturing schemes, J. Comput. Phys. 77 (1988) 439–471.
[20] J. Yan, C.-W. Shu, A local discontinuous Galerkin method for KdV type equations, SIAM J. Numer. Anal. 40 (2) (2002) 769–791.
[21] J. Yan, C.-W. Shu, Local discontinuous Galerkin methods for partial differential equations with higher order derivatives, J. Sci. Comp. 17 (2002) 27–47.
[22] M. Zhang, C.-W. Shu, An analysis of three different formulations of the discontinuous Galerkin method for diffusion equations, Math. Model. Meth. Appl. Sci. 13 (2003) 395–413.